American Mineralogist, Volume 75, pages 1381–1398, 1990

Homogenizing rhyolitic glass inclusions from the Bishop Tuff

CHRISTINE M. SKIRIUS, JONATHAN W. PETERSON,* ALFRED T. ANDERSON, JR.
The Department of the Geophysical Sciences, The University of Chicago, Chicago, Illinois 60637, U.S.A.

ABSTRACT

Silicate glass inclusions can be homogenized to a single glassy phase free of bubbles and crystals by heating to near magmatic temperatures at near magmatic pressures. Variably devitrified glass inclusions in quartz phenocrysts from the plinian ash-fall pumice and four of the five ash-flow units of the Bishop Tuff were heated in an internally heated gas pressure vessel to 800 or 900 °C at ~2 kbar for approximately 20 h and quenched nearly isobarically. The heating procedure yielded glassy, unfractured inclusions free of crystals and gas bubbles for most inclusions. Some extensively devitrified inclusions with lower H_2O content required heating at higher temperature (≥900 °C) for complete homogenization. Inclusions that were intersected by cracks prior to heating do not revitrify owing to loss of volatiles, possibly during posteruptive cooling. Spectroscopic analyses of homogenized inclusions reveal a small range in concentrations of H_2O and CO_2 that is within the larger range found for stratigraphically equivalent natural, unheated inclusions. Detailed comparisons of the most equivalent inclusions from the same pumice clast or closely similar ones reveal slightly less H_2O in heated inclusions. These facts are interpreted to signify that few or no volatiles leak from inclusions during heating but that the speciation and absorptive properties of H_2O may be slightly dependent upon quenching history.

INTRODUCTION

As quenched samples of magmatic melt, silicate glass inclusions in volcanic phenocrysts can provide information on the preeruption concentrations of dissolved volatiles in magma. Dissolved H_2O (molecular), OH^-, and CO_2 (molecular) have been determined by Fourier transform infrared (FTIR) spectroscopy on spots as small as a few tens of micrometers in diameter in glassy inclusions in quartz phenocrysts (Anderson et al., 1989; Skirius, 1989) and olivine (Anderson and Skirius, 1989). Such determinations of H_2O and CO_2 dissolved in glass inclusions in phenocrysts as well as in other natural glasses (Newman et al., 1988) and experimental glasses (Newman et al., 1986; Stolper et al., 1987; Silver and Stolper, 1989; Silver et al., 1990) can lead to important conceptual progress in volcanology and petrology.

Vapor bubbles and devitrification in glass inclusions present unique problems to the measurement of dissolved volatiles by spectroscopy. Initially dissolved H_2O and CO_2 in the trapped melt may be redistributed into vapor bubbles and hydrous minerals that form during cooling. Consequently, a variable concentration of volatiles may exist in the glass. The spectroscopically measured concentrations of H_2O and CO_2 remaining dissolved in the glass of such inclusions may thus differ from the original concentrations in the trapped melt. Extensively devitrified glass inclusions are opaque owing to abundant crystallites and cannot be analyzed by transmission spectroscopy.

In order to overcome these problems, we have developed a procedure to homogenize inclusions. By heating inclusions in quartz phenocrysts from the Bishop Tuff at moderate pressure, we were able to dissolve crystals and gas bubbles and produce glassy, unfractured inclusions. This procedure avoids decrepitation, which can be an effect of homogenization experiments done using a microscope heating stage (Sommer, 1977; Beddoe-Stephens et al., 1983). Earlier work on homogenizing silicate glass inclusions (Clocchiatti, 1975; Roedder, 1984, p. 474, 479–482 and references therein) has focused on obtaining the temperature of trapping (i.e., crystallization temperature of the host) and the sequence of phase changes upon laboratory heating and cooling. Although such information may be derived from our experiments, we focus on restoring devitrified and bubble-bearing inclusions to a homogeneous glass that is uniform with respect to H_2O and CO_2 concentrations without volatile loss.

Whether volatile loss occurred during the heating experiments was evaluated by spectroscopically measuring the H_2O and CO_2 contents of homogenized inclusions and comparing these results with those of unheated inclusions. Ideally, the comparison should be made using the same inclusion. However, this direct comparison is not possible for one of the following reasons: (1) The spectroscopic measurement of volatiles before heat treatment cannot be made on opaque inclusions. (2) The inclusion must be completely enclosed (unsectioned) within the quartz crystal during heating in order to avoid the loss of volatiles or the rupture and decrepitation of the

* Present address: Amoco Production Company, 501 Westlake Park Boulevard, P.O. Box 3092, Houston, Texas 77253, U.S.A.

0003–004X/90/1112–1381$02.00

inclusion. This would require that the initial measurement be made on an enclosed inclusion. The concentrations of H_2O and CO_2 measured for enclosed inclusions are uncertain because of nonuniform inclusion thickness and refraction of light at inclusion-quartz boundaries. Such uncertainty might obscure differences in volatile concentration that might be attributed to the heating procedure. Therefore, we first heated enclosed inclusions and then doubly polished them prior to spectroscopic analysis. The H_2O and CO_2 concentrations of homogenized (artificially heated and doubly polished) inclusions were compared with those of similar-looking, naturally glassy or partly devitrified doubly polished inclusions either from the same pumice clast or from stratigraphically similar pumice clasts.

Geologic context of samples

The samples used in this study are from the 0.7 m.y. Bishop Tuff of eastern California (Bailey et al., 1976; Hildreth, 1977, 1979). It is a voluminous high-silica rhyolite that was emplaced during collapse of the Long Valley caldera and consists of erupted material representing a range of cooling histories and volatile contents.

The tuff is made up of a basal, plinian ash-fall pumice deposit and five major ash-flow tuff emplacement units or lobes. The Chidago, Gorges, and Tableland lobes, along with the plinian ash-fall pumice unit, make up a distinguishable stratigraphic sequence to the east and southeast of the caldera rim and are referred to here as the early-erupted, lower temperature units (720–763 °C) based on Hildreth (1979). The Adobe Valley and Mono Basin ash-flow lobes are referred to as the higher temperature (760–790 °C) units and are considered to have been last emplaced. These ash-flow units are north of the caldera, and, although they overlie some lower temperature material, they show no direct stratigraphic relation to the low-T units to the east and southeast (Hildreth, 1979).

Fresh, vitric pumice is abundant and occurs as frothy, white-gray pieces of ~5 cm in the ash-fall pumice deposit and as larger blocks in the ash flows. Quartz and sanidine are the most abundant phenocryst minerals. Glass inclusions are present in most quartz phenocrysts.

Glass inclusion textures and cooling rate

Homogeneous silicate melt trapped as primary inclusions in phenocrysts during crystal growth may be completely glassy or contain one or more daughter (secondary) phases (crystals and vapor bubbles) at room temperature. Although the daughter phases present are a function of bulk composition, inclusion size, cooling rate, and quenching temperature (Roedder, 1979, 1984), cooling rate is probably a main factor for volcanic samples (e.g., Payette and Martin, 1986). Melt inclusions rapidly quenched in heating experiments freeze to a glass free of bubbles and crystals (Sobolev et al., 1972; Kozlowski, 1981). Similarly, the absence of bubbles and devitrification in large, rounded, glassy inclusions in quartz phenocrysts from the plinian ash-fall pumice of the Bandelier Tuff and from the Toba Tuff are interpreted to reflect rapid quenching upon eruption (Sommer, 1977; Beddoe-Stephens et al., 1983). Such inclusions have quite likely undergone little posteruptive modification. Most inclusions derived from overlying ash-flows, however, have vapor bubbles and are variably devitrified. In addition, some ash-flow inclusions have negative crystal shapes, are texturally zoned, heavily vesiculated, or cracked (Sommer, 1977; Anderson et al., 1989). The prevalent devitrification and bubble formation seem best explained by relatively slow cooling within thick ash-flow sheets that would allow time for nucleation and growth of secondary crystals and bubbles. Cracked inclusions possibly formed during (Bacon et al., 1988, 1990) as well as after extrusion.

Methods

Samples

Individual pumice clasts were collected from the plinian ash-fall deposit and from nonwelded portions of four of the five major overlying ash-flow lobes (Chidago, Gorges, Adobe Valley, and Mono Basin). Pumice clasts taken from the same stratigraphic position within a particular eruptive unit are considered to have experienced a similar cooling rate after deposition. A total of 16 pumice samples were used in this study, and most consist of a single pumice clast. In order to separate crystals, pumice clasts were gently crushed and the bulk of the glass floated in H_2O. The crystal separate was immersed in refractive index liquid ($n \approx 1.54$, close to that of quartz) held in a watch glass to aid in viewing inclusions. Forceps and a dissecting microscope were used to hand-pick quartz phenocrysts with uncracked, enclosed inclusions. Picked crystals were placed in a retaining well, glued to a glass slide, and filled with $n = 1.54$ refractive index liquid. A petrographic microscope was used to study and document photographically selected inclusions and host crystals. Microscopic study prior to and following the heating experiments established equivalence between heated and unheated inclusions.

The inclusion glasses are uniformly high-silica rhyolite (typical plinian inclusion analysis: 77 wt% SiO_2, 12 wt% Al_2O_3, 0.6 wt% FeO, 0.03 wt% MgO, 0.4 wt% CaO, 4.0 wt% Na_2O, 4.6 wt% K_2O) and are similar to Hildreth's (1977) whole-rock analyses for plinian pumice. Little variation in major-element composition exists between the plinian and the late, high temperature Mono Basin samples (see also Anderson et al., 1989).

Homogenization experiments

Crystals with inclusions were placed into loosely crimped Pt tube segments of 2.3 mm (od) and heated in an internally heated Ar pressure vessel (IHPV) (design after Holloway, 1971) to 800 °C or 900 °C at ~2 kbar for approximately 20 h. Loosely crimping the capsule, instead of sealing it, allowed the crystals to be in direct contact with an atmosphere of dry Ar gas having a very

low H_2O vapor pressure (less than ~0.1 bar). It also prevented collapse of the capsule, thereby ensuring that crystals would not be crushed and could be poured out of the capsule at the end of an experiment. The *P-T* conditions were chosen to approximate the estimated conditions of crystallization of Bishop Tuff ash-flow phenocrysts (<800 °C by Fe-Ti oxide equilibria, Hildreth, 1979; ~2.3 kbar gas saturation pressure for the high-*T* Mono Basin lobe, Anderson et al., 1989). An experiment duration of 20 to 24 h was found to be adequate to ensure complete resorption of bubbles and crystals in most inclusions. According to diffusivity measurements of Watson et al. (1982) for CO_2 ($D_{CO_2 800\ °C} = 10^{-9}$ cm²/s for anhydrous silicic melt), a spherical inclusion 100 μm in diameter would become uniform with respect to CO_2 concentration in about 1 d in our experiments. Considering that the diffusivity of H_2O in rhyolitic glass (Karsten et al., 1982) is 1–2 orders of magnitude greater than that for CO_2, one would expect that H_2O concentration gradients would also be eliminated during experiments of this length.

Samples in the IHPV were initially brought to a cold Ar gas pressure of approximately 1.5 kbar, then heated to the desired temperature. Heating the confined Ar gas brought the pressure to the desired value. The selected pressure (~2 kbar) was always attained before the desired final temperature of 800 °C or 900 °C; this allowed nearly isobaric heating of samples above about 300 °C. Pressures were measured simultaneously with an Astra bourdon tube gauge and a manganin cell, both of which were calibrated against a Heise bourdon tube gauge. Pressures are considered accurate to within 50 bars. Temperatures were measured by two Inconel-sheathed, chromel-alumel thermocouples 6 mm apart at the ends of the Pt tube segment that contained the crystals. The cold junction of the thermocouple was laboratory temperature and was measured after each experiment. The temperature gradient across the capsule was usually less than 20 °C and often less than 10 °C. Temperature was controlled to within one degree by an electronic, solid-state controller, and reported temperatures are considered accurate to ±10 °C. No temperature correction was made for pressure-induced emf, which should be negligible at the *P-T* conditions of our experiments (Getting and Kennedy, 1970). At the end of an experiment, the sample was quenched nearly isobarically by switching off power to the heat source. This gave an approximate quench rate of 5 °C/s measured from the hot thermocouple for one experiment. Quenched samples thus attained the quartz inversion temperature (~573 °C) in about 40 s.

Infrared spectroscopy

Sample preparation. Quartz phenocrysts were mounted in acetone soluble cement (General Fiber Optics Inc.) on microscope slides for grinding and polishing. The transparent cement ($n \approx 1.54$) has a softening point of ~55 °C, which enabled several crystals to be individually positioned on the same slide with slight rewarming on a hot plate. Each crystal was oriented on the microscope slide so that the maximum number of large inclusions would lie in a plane parallel to that of the glass slide and thus be intersected during grinding. Doubly polished crystal plates (with inclusions intersected on both sides) were prepared by hand-grinding on 600-grit paper rinsed with H_2O and then polishing with 6-μm and 1-μm diamond paste (Metadi compounds, Buehler Ltd.), using cutting fluid (Isocut, Buehler Ltd.) as a lubricant.

After one side of an inclusion was polished, the slide was warmed to soften the cement, and the crystal was turned over with forceps and pressed flush to the glass slide while viewed with a dissecting microscope. The grinding and polishing procedure was then repeated for the second side. Although naturally cooled inclusions are relatively strain-free and survive sectioning well, many reheated (lab-quenched) quartz crystals show strain birefringence around inclusions and commonly shatter or crack during final polishing.

It is important to produce doubly polished inclusions with two parallel polished surfaces to ensure constant inclusion thickness and to minimize refraction and scattering of the infrared beam at inclusion-air interfaces. Uniform thickness can be monitored during grinding by observing the distribution of interference colors in the host crystal when viewed between crossed polarizers. Doubly polished samples were removed from the mount by warming the cement, picking the crystals out, and dissolving the adhering cement in acetone. Crystals were given a final rinse in toluene or acetone prior to spectroscopic analysis.

Infrared spectroscopy. FTIR spectroscopy was used to measure total H_2O (as the sum of molecular H_2O and OH^-) and CO_2 in glass inclusions in the wavelength range 1.3–8.0 μm (7500–1250 cm^{-1}). Analyses were performed by placing an inclusion contained in a wafered quartz crystal over a pinhole aperture in order to direct the beam path through the inclusion. Depending on the size of the inclusion, pinhole apertures of either 50 or 100 μm diameter were used to contain the beam within the interior of the inclusion. Aperture sizes smaller than 50 μm resulted in poor quality spectra in most cases.

Analyses were performed on Nicolet 60SX spectrometers at the California Institute of Technology using the regular sample compartment, CaF_2 beamsplitter, and InSb detector, and at the University of Chicago using the microbeam chamber, KBr beamsplitter, and HgCdTe (MCT-A) detector. The microbeam is an optional auxiliary beam for the Nicolet instrument that uses stepper motor-controlled beam-condensing mirrors to achieve f1 optics useful for the analysis of very small samples (Nicolet Operations Manual, 1986). Analyses done on the same samples using both instrumental arrangements gave results that agreed to within <2%. Precision and accuracy of the method are discussed by Newman et al. (1986, 1988) and Silver and Stolper (1989). We estimate that the typical uncertainty in concentration for H_2O is a few percent of the amount (±~0.15 wt% absolute) and CO_2 is about 10% of the amount reported (±~5–20 ppm). Reproduc-

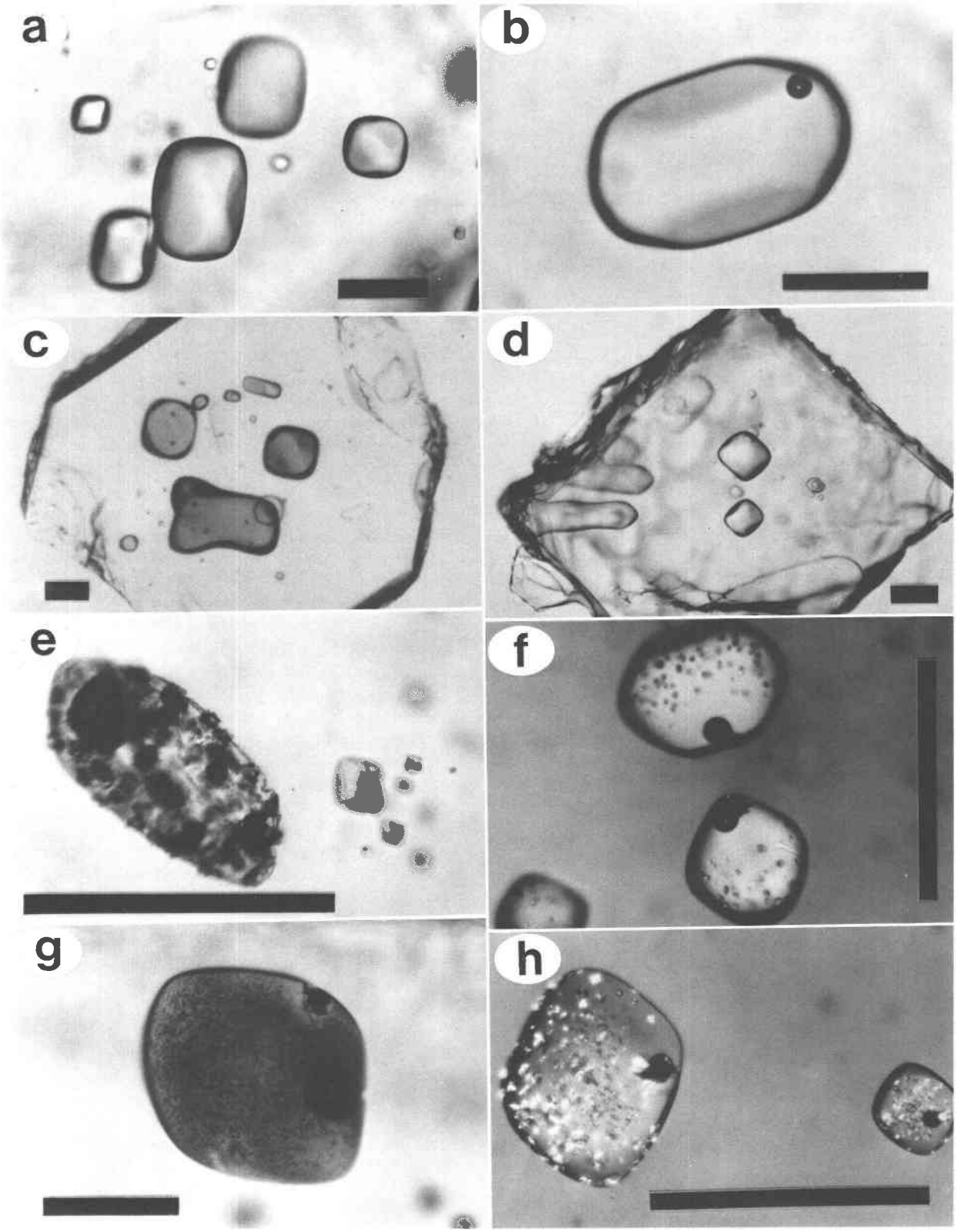
a
b
c
d
e
f
g
h

ibility (i.e., precision) of absorbance measurements is good, with differences of band intensities (after subtraction of background) between repeated measurements on the same inclusion usually ≤ 0.002 absorbance units for the H_2O bands and not exceeding 0.01 for the CO_2 band.

The spectrometer and sample chamber were continuously purged with dry N_2 to reduce background noise, especially in the region of the CO_2 band, because CO_2 concentrations in the sample are at the ppm level. A routine procedure of purging for 12 min was followed after opening the sample chamber to room atmosphere. Best results were achieved by leaving the lid to the sample chamber slightly ajar when taking background and sample spectra to allow an escape for outward flow of gas and more efficient flushing of the system. Adherence to this purging procedure was found to be critical in producing reproducible spectra.

Spectra obtained in the wavelength region 7500 cm^{-1}–3500 cm^{-1} for H_2O and 2800 cm^{-1}–2000 cm^{-1} for CO_2 were plotted as linear absorbance (base ten logarithm) vs. wavenumber on chart paper. Absorbance intensities of the three bands studied (5200 cm^{-1}, H_2O mol; 4500 cm^{-1}, OH^-; and 2350 cm^{-1}, CO_2) were taken as the peak heights measured directly from a plotted spectrum after drawing a curved or straight background that is tangent to the spectrum on either side of each peak. This is the same graphical background-subtraction procedure employed by Newman et al. (1986). Band assignments are those of Newman et al. (1986) for H_2O species and Fine and Stolper (1985) for CO_2.

The peak absorbances are related to concentration by Beer's law, which can be written as $c = (\text{mol wt} \times abs.)/(\rho \times d \times \epsilon)$ where c is the concentration in weight fraction, mol wt is the molecular weight (18.02 and 44.00 for H_2O and CO_2, respectively), *abs.* is absorbance which is dimensionless, ρ is density in g/L, d is path length (inclusion thickness) in centimeters, and ϵ is the molar absorption coefficient or molar absorptivity in L/(mol·cm). We used molar absorptivities of 1.61 ($\pm$ 0.05) and 1.73 ($\pm$ 0.02) L/(mol·cm) for the H_2O (molecular) band at 5200 cm^{-1} and the OH^- band at 4500 cm^{-1}, respectively, determined by Newman et al. (1986) and verified by Silver et al. (1990) for synthesized rhyolitic glasses with up to 4 wt% H_2O. The molar absorptivities for molecular H_2O and OH are defined in terms of the amount of H_2O that would be released from the sample if all of the H contributing to a given band were converted to H_2O (Newman et al., 1986). A molar absorptivity of 945 ($\pm$ 45) L/(mol·cm) was used for the molecular CO_2 band at 2350 cm^{-1}, as determined by Fine and Stolper (1985) for sodium aluminosilicate glasses. A value of 2280 g/L was used for the density of rhyolitic glass.

Inclusion thickness was determined by mounting the polished crystal on a needle and immersing it in a low cylindrical well filled with oil having a refractive index close to that of quartz ($n \approx 1.54$). This allowed the crystal to be rotated and viewed on its edge so that inclusion thickness could be measured microscopically with a calibrated eyepiece. Most inclusions are on the order of 100 μm thick. For inclusions near the edge of the crystal, measurements are considered to be accurate to within 1 μm; inclusions centrally located within the crystal are more poorly resolved, and thicknesses are believed to be accurate to $\pm$ 3–4 μm. In most cases, thickness measurements made in this way agreed with measurements made using a digital micrometer (543 Series Digimatic Indicator, Mitutoyo Mfg. Co., Ltd.). However, the digital micrometer with flat anvils measures only the maximum thickness of slightly wedge-shaped or dirty crystals, whereas the visual method is able to measure any variation in thickness of inclusions contained along the entire length of the crystal. Such variation in thickness becomes important for thin samples ($\sim$50 μm) where uncertainty of a few micrometers gives an error of several tenths of a percent in H_2O concentration. More confidence is placed on the first method because a visual assessment of the inclusion thickness can be made directly.

Results

The results of textural observations of inclusions before and after the heating experiments are shown in Figures 1–6 and are described below. Figure 1 shows some textural features of Bishop Tuff glass inclusions from pumices within the plinian deposit (Figs. 1a–1c), early ash flows (Figs. 1d and 1e), and Mono Basin ash flow (Figs. 1f–1h) before heating. Additional textural features for in-

←

Fig. 1. Bishop Tuff glass inclusion textures before heating (100-μm scale bar). **(a)** Typical glassy inclusions in quartz from plinian ash-fall pumice. **(b)** Plinian inclusion with one small vapor bubble 18 μm in diameter. **(c)** Doubly polished plinian quartz crystal (sample 6B-D3) containing several large, green, glassy inclusions with a few tiny birefringent crystal clusters (dark specks in inclusions). The smaller inclusions in this crystal each has a vapor bubble. **(d)** Unpolished euhedral quartz phenocryst from the Chidago ash flow containing two large, partly faceted, glassy inclusions. The glass-filled reentrants visible at one apex of the crystal are also common textural features in plinian and early ash-flow quartzes. **(e)** Coarsely crystalline devitrification is exemplified by these inclusions from a Gorges ash-flow pumice (sample 133A). The largest inclusion has an irregular boundary and a vapor bubble near its upper end. Partly devitrified inclusions from the Mono Basin ash flow (pumice LV81-17A) are shown in **f**, **g**, and **h**: **(f)** Partly faceted inclusions commonly have one bubble at one apex of the bipyramid and a zone of fewer devitrification crystals in the glass surrounding the bubble (crossed polarizers). **(g)** Inclusion with abundant finely dispersed crystallites and one large vapor bubble. **(h)** Inclusions showing birefingent crystalline devitrification, some attached to a bubble (crossed polarizers).

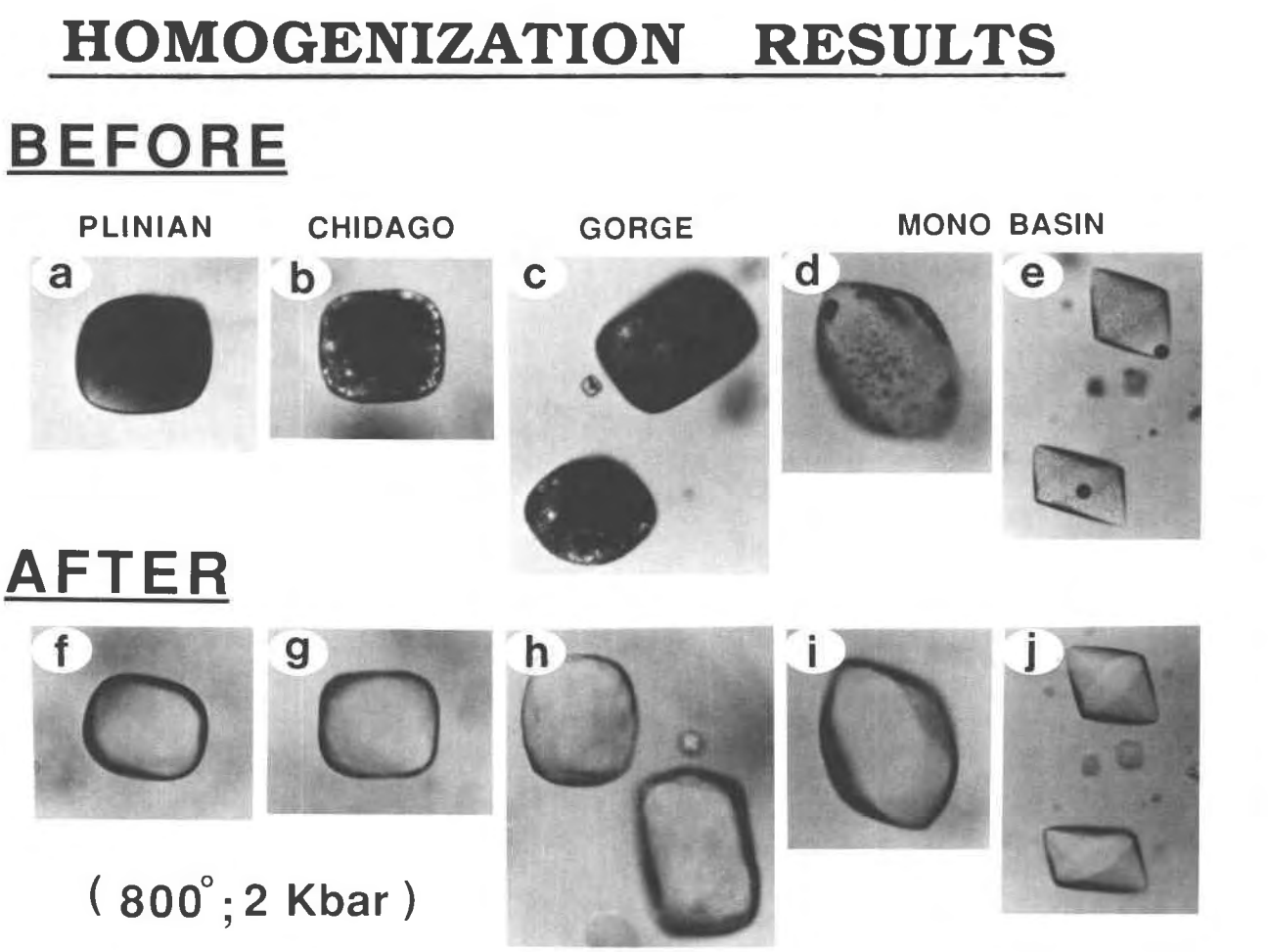

Fig. 2. Results of the homogenization experiments. Examples of variously devitrified inclusions from four major eruptive units of the Bishop Tuff (see Table 1) are (**a**) inclusion 6B-G5, (**b**) inclusion 16-H5, (**c**) inclusion 24-C3, (**d**) inclusion LV81-17A-2, (**e**) inclusion LV81-17A-1. The same inclusions after heating to 800 °C at 2 kbar for ~20 h are shown in **f–j**. The homogenized (revitrified) inclusions are completely glassy, uncracked and unchanged in size and shape. (Inclusion in **a** is 100 μm in length; all other photos are at the same scale. The apparent smaller size of the inclusion in **f**, compared with **a**, is an artifact of orientation.)

clusions from these units before heating are shown in Figures 2a–2e, 3a and 3b, 4a, and 5a. Figures 2f–2j, 3c–3f, 4b, and 5b also show the appearance of the corresponding inclusions following the heating procedure. A collection of variously cracked Mono Basin ash-flow inclusions is shown in Figure 5. Textures of incompletely homogenized Mono Basin ash-flow inclusions with protruding vapor bubbles are shown in Figures 6a–6c.

Observations of Bishop Tuff glass inclusions before heating

Plinian inclusions. Glass inclusions in plinian quartz phenocrysts are abundant and typically ~50–>300 μm in diameter, rounded to partly faceted in shape, clear and glassy (Fig. 1a). Bubbles are uncommon and typically occur in the larger inclusions within a crystal. Most bubbles are near or attached to the wall (Fig. 1b). Bubble size (<0.5 vol% of inclusion) correlates well within inclusion size. Inclusions with more than one bubble are rare (~1% of all bubble-bearing inclusions). Most glassy inclusions that are intersected by a crack in the quartz host contain several large bubbles.

Most plinian sanidine phenocrysts have a few small glass inclusions, but most are cracked and contain several vapor bubbles. Sanidines with large (~100 μm) uncracked glassy inclusions are rare and show conspicuous strain birefringence adjacent to the inclusion. The inclusion and surrounding sanidine usually shatter during sample polishing. As a result, few spectroscopic analyses have been made on inclusions in sanidine.

Phenocrysts from most plinian pumices contain clear, glassy, bubble-free inclusions. In some pumice clasts, however, inclusions have unusual textural features, such as more abundant vapor bubbles, cracks, or colored glass. For example, glassy inclusions from pumice clast 6B vary from pale olive green (Fig. 1c) to dark brown and show varying degrees of incipient devitrification from crystal to crystal. All inclusions within a particular crystal, however, are devitrified to a similar extent. Dark-colored glassy inclusions have a cloudy appearance due to the

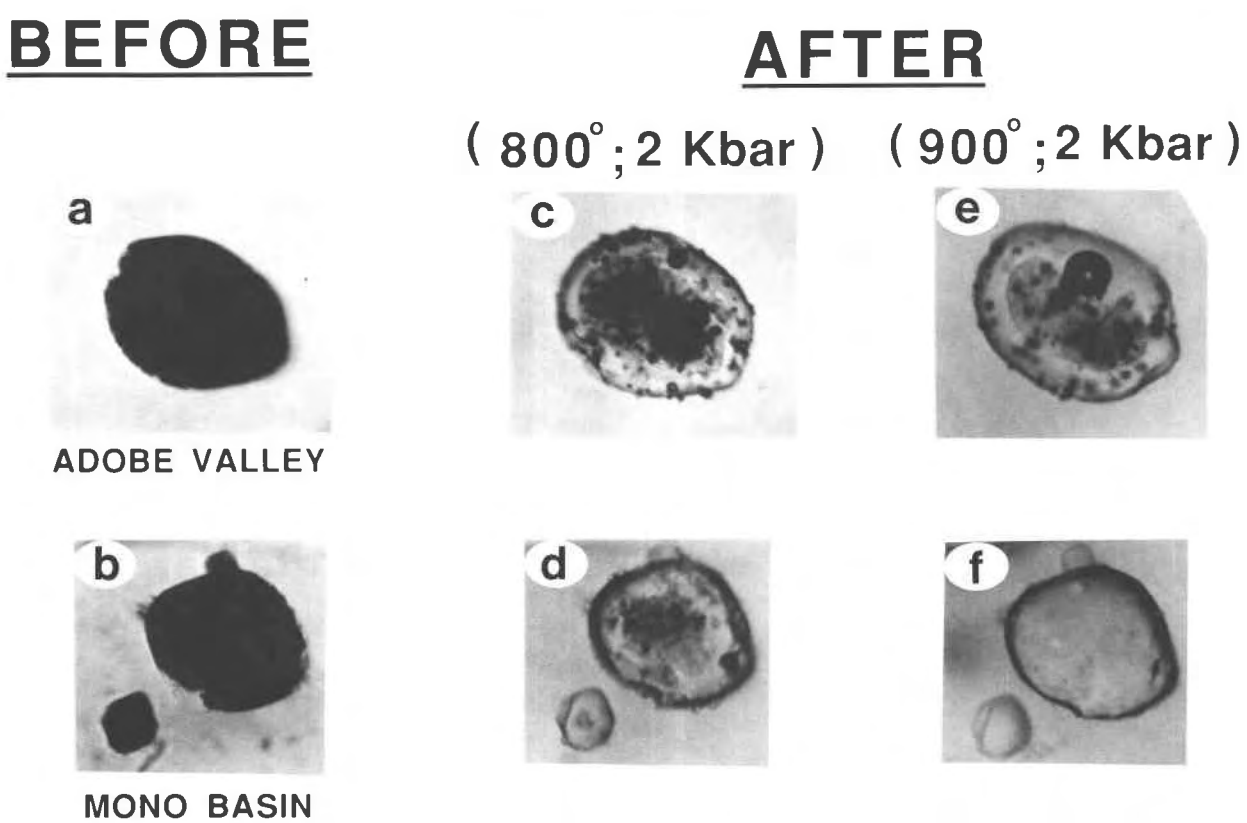

Fig. 3. Examples of extensively devitrified inclusions from the (**a**) Adobe Valley and (**b**) Mono Basin ash-flow units (inclusion 42-3) that were incompletely revitrified in the homogenization experiments at 800 °C and 2 kbar. The inclusions retained a birefringent crystalline core and crystals and vapor bubbles along the wall (**c**) and (**d**). Heating to 900 °C in a subsequent experiment resulted in (**f**) complete homogenization (dissolution of crystals and vapor bubbles) for the Mono Basin inclusions, but the Adobe Valley inclusion (**e**) remained only partially revitrified. (Larger inclusions are 120 μm long.)

presence of very fine-grained crystals (<1 μm) and, possibly, vapor bubbles dispersed throughout the glass (Fig. 2a). Some pale-colored inclusions, although clear and glassy, contain clusters of highly birefringent crystals (~10 μm diameter) unusual for plinian inclusions in general. In addition, vapor bubbles occur in small inclusions (10–20 μm diameter) as well as large ones. Colored glass inclusions also occur in certain early ash-flow pumice samples and appear to be clast-specific.

Early ash-flow inclusions. Glass inclusions in quartz phenocrysts from several pumice clasts from the early-erupted Chidago ash-flow lobe are texturally similar to most plinian inclusions: they are large, rounded to partly faceted, clear and glassy, with or without one or more small vapor bubbles (Fig. 1d). There is, however, more diversity in the degree of inclusion devitrification among crystals from different clasts of pumice collected in the Chidago ash-flow lobe. The degree of devitrification appears to be specific to a particular pumice clast, rather than stratigraphically controlled.

The two pumice samples studied from the Gorges lobe contain only devitrified inclusions, but these are otherwise similar in size and shape to the Chidago and plinian inclusions. Some devitrified inclusions are texturally zoned with a coarsely crystalline birefringent rim along the inclusion wall and a central region containing bubbles and tiny crystals (Fig. 2b). Such textures have been described for ash-flow inclusions from the Bandelier Tuff (Sommer, 1977) and Toba Tuff (Beddoe-Stephens et al., 1983). Other extensively crystallized inclusions contain large, irregularly shaped bubbles throughout. Smaller inclusions (10–30 μm) have a vapor bubble but appear less crystallized than larger inclusions within the same crystal. Large, cracked inclusions commonly are glassy and partly vesiculated.

The boundaries between devitrified inclusions and quartz host may be smooth and sharp or slightly bumpy and irregular in outline. A small amount of quartz crystallization on the inclusion wall is sometimes obvious because quartz extends inward from the original wall and partially encloses daughter minerals. An irregular inclusion wall is especially evident for some Gorges (133A) inclusions. These inclusions have one or more large bubbles and coarse, patchy birefringent crystallization—some of which is partly embedded in a discontinuous layer of quartz growth 1–3 μm thick (Fig. 1e).

Mono Basin and Adobe Valley ash-flow inclusions. All uncracked glass inclusions from these highest temperature ash-flow units are at least partially devitrified. They are typically less abundant, smaller ($\lesssim$150 μm diame-

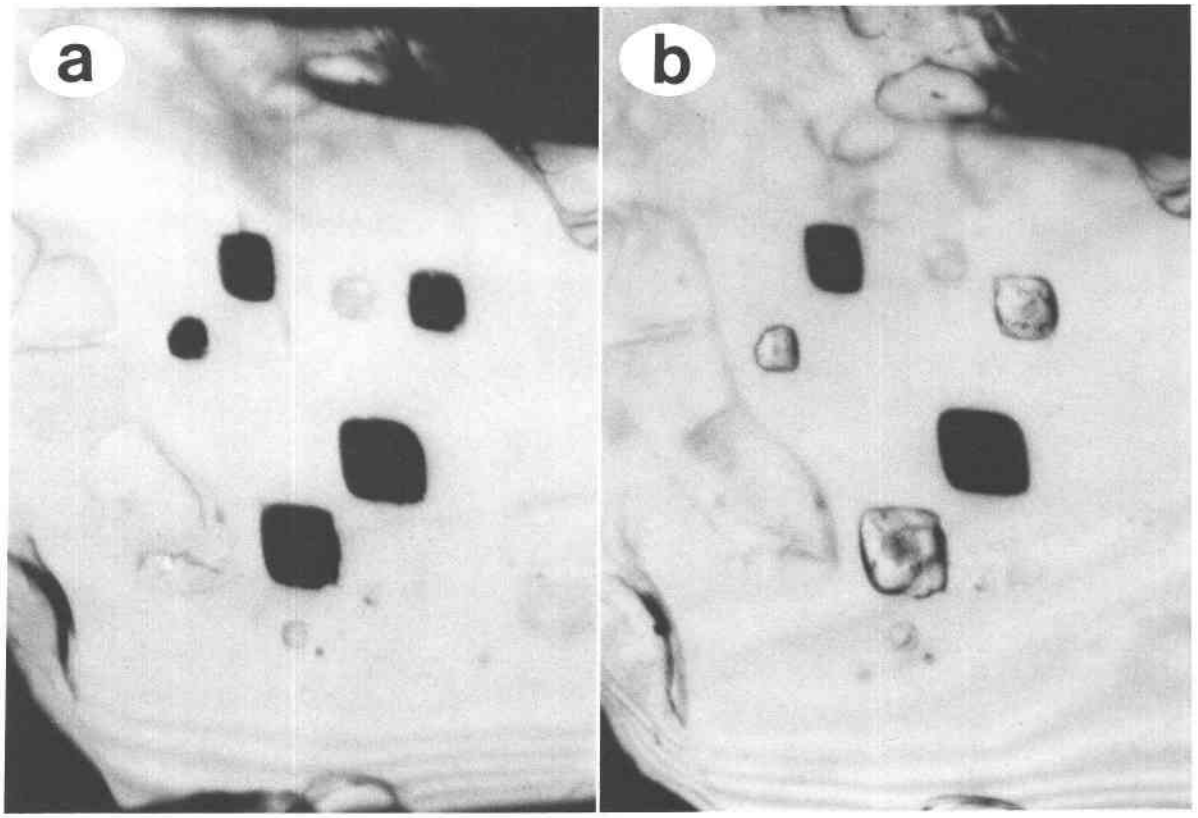

Fig. 4. (**a**) A Mono Basin ash-flow quartz crystal containing several extensively devitrified negative crystal inclusions before heating. Note crack in quartz intersecting the larger inclusion at the upper left. The crack also extends to the lower right and intersects the central inclusion. (**b**) Same crystal after heating. The two cracked inclusions remain unaffected because of volatile loss, whereas the other uncracked inclusions in the crystal revitrify. (Larger inclusions are 100 μm long.)

ter), and more angular (faceted) than inclusions from the lower temperature units. Most inclusions of all sizes are completely opaque with little or no glass remaining and have pronounced bipyramidal negative crystal shapes (Fig. 4a). Inclusion boundaries of many are irregular (Figs. 3a and 3b). Many large inclusions have cracks radiating short distances from the apices of the inclusion into the quartz host (Fig. 5a). Ash-flow quartz phenocrysts are commonly broken or internally cracked, possibly caused in part by sample preparation. Accordingly, many devitrified inclusions are intersected by penetrative cracks in the quartz host (Figs. 5c–5e). Glassy inclusions are rare and contain large gas bubbles (Fig. 5f), and virtually all are visibly cracked.

Two pumice clasts from the Mono Basin ash flow (LV81-17A and LV81-18A) differ from others in having inclusions that are only partially devitrified. Most inclusions are colorless glass containing abundant crystallites and one or more vapor bubbles (Figs. 1f–1h). The walls of some inclusions have clusters of birefringent acicular or dendritic crystals of biotite or smectite 1–10 μm long (Fig. 1h) (Anderson et al., 1989). Similar crystals are attached to some vapor bubbles (Figs. 1f, 1h, 2d). The shapes of inclusions vary from rounded, partly faceted outlines (Fig. 1g) to pronounced negative crystal bipyramids (Fig. 2e). Unlike the more devitrified negative crystal inclusions from the majority of Mono Basin pumices, the largely glassy inclusions from the 17A and 18A samples are rarely cracked.

Results of homogenization experiments

The experimental conditions for all successfully homogenized inclusions are given in Table 1. Also noted in Table 1 are characteristic textural features of the glass inclusions prior to heating.

Plinian and early ash-flow inclusions. As a result of heating, vapor bubbles and devitrification products completely dissolve and inclusions are homogeneously glassy, clear, and uncracked, as shown in Figure 2f–2h. All experiments for these samples were done at 800 °C and about 2 kbar pressure for 10–22 h. Colored glass inclusions became colorless following the heating procedure. Inclusion sizes and shapes are unaffected (a 5% change in linear dimension would be obvious). Those that initially had an irregular outline retain a bumpy inclusion wall after heating. A glassy plinian inclusion of ~180 μm diameter that contained two vapor bubbles prior to heating afterward no longer had vapor bubbles. Although intact,

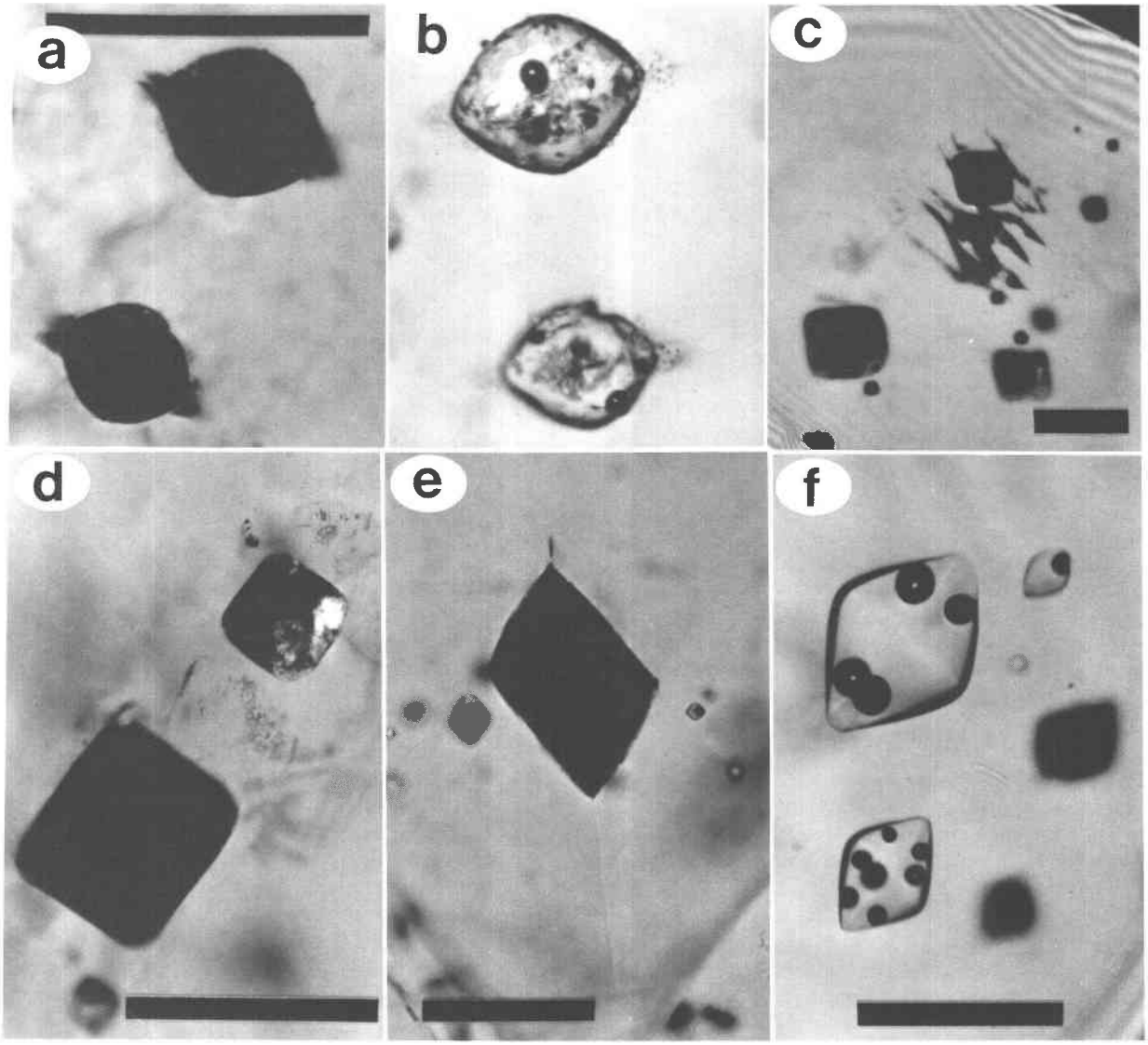

Fig. 5. Cracked inclusions (100-μm scale bar). (**a**) Two devitrified (opaque) inclusions showing dark localized cracks in the surrounding crystal. The cracks are likely caused by the sudden 1 vol% shrinkage of quartz upon inversion during cooling. (**b**) The same two inclusions as in **a** after heating to 800 °C and partial revitrification. Inclusions intersected by penetrative cracks in the quartz host are shown in **c**, **d**, **e**, and **f**. (**c**) An extensive crack made visible by internal reflection of transmitted light. Viewed at a slightly different angle, the crack would not be obvious. (**d**) A crack parallel to the plane of focus is decorated with tiny vapor bubbles and intersects both inclusions. (**e**) A crack projecting from the apicies of this inclusion with negative crystal form extends downward in the photo to the edge of the crystal. (**f**) A group of three inclusions that were cracked early in their cooling history to allow partial vesiculation of the melt (and volatile loss). Inclusions shown in **c–f** were unchanged in appearance after heating. The devitrified (opaque) inclusions in **f** were revitrified.

the homogenized inclusion was intersected by a crack in the quartz that radiated from the inclusion. Some quartz crystals with large, initially glassy inclusions without vapor bubbles separated into pieces along cracks intersecting the inclusions. Such inclusions that were intersected by cracks or had broken apart as a result of the heating procedure may have lost volatiles and were not analyzed spectroscopically.

Mono Basin and Adobe Valley ash-flow inclusions. The partially devitrified inclusions from pumice clast LV81-17A (Figs. 2d and 2e) were homogenized to a glassy phase free of bubbles and crystals at 800 °C and 2 kbar for 20 h (Figs. 2i and 2j), with one exception (LV81-17A-3; see Table 1). Inclusions of all sizes were revitrified and otherwise unchanged in size and shape. Inclusions intersected by a crack in the quartz host prior to heating (Fig. 4a) remain unaffected afterward (Fig. 4b). Rare glassy inclusions containing several bubbles (Fig. 5f) and devitrified

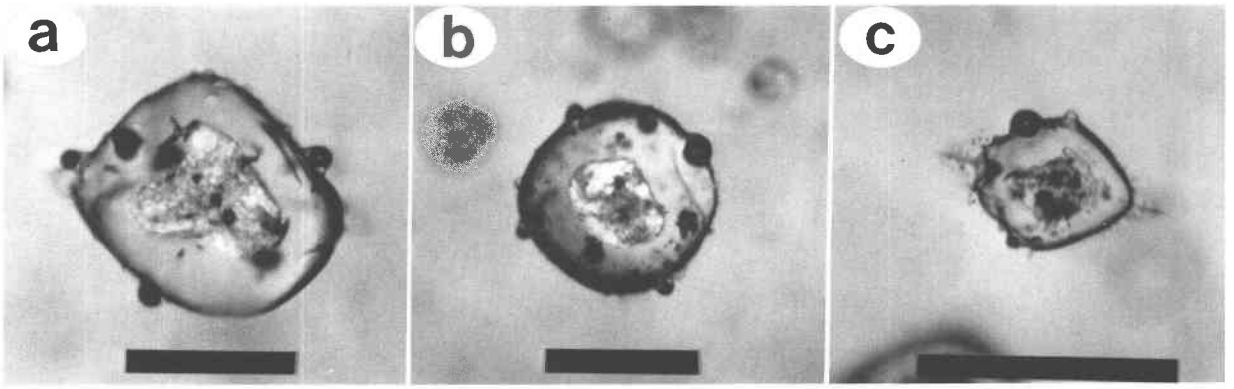

Fig. 6. Examples of protruding bubbles in incompletely homogenized inclusions from the Mono Basin ash flow [(**a**) and (**b**), from pumice sample 32W; (**c**), sample 41; 100-μm scale bar]. The vapor bubbles in these inclusions protrude 6–14 μm into the quartz from a smooth (**b**) or an irregular, bumpy inclusion wall (**a** and **c**). The vapor bubbles are thought to have locally enhanced dissolution of quartz ahead of the bubble, thereby drilling themselves into the surrounding crystal (see discussion). Upon further heating at higher temperature, the vapor bubbles dissolve and the walls of the inclusions become less bumpy.

inclusions in sanidine phenocrysts also could not be homogenized (i.e., bubbles and crystals remained virtually unaffected by heating).

Extensively devitrified (opaque) inclusions from four other Mono Basin pumice clasts (32W, 41, 42, 45) and two Adobe Valley pumices were only partially revitrified at the above experimental conditions. These inclusions retained a birefringent polycrystalline core, clusters of tiny, highly refractive acicular crystals, and vapor bubbles along the wall (Figs. 3c and 3d). The vapor bubbles protrude 6–14 μm into the quartz from an irregular, bumpy inclusion wall, as also shown for three other Mono Basin inclusions in Figures 6a–6c.

Mono Basin inclusions which did not homogenize after initial attempts at 800 °C were successfully homogenized by heating at 900 °C and 2.2 kbar for 24 h in either a second or third experiment (e.g., Fig. 3f; see notes of Table 1). In some of these inclusions, however, a few tiny crystals remained along a slightly bumpy inclusion wall.

Heated Adobe Valley inclusions either had initial cracks and remained unchanged after heating or were only partially revitrified even at 900 °C, as shown in Figure 3e. As a result, no Adobe Valley inclusions were analyzed for H_2O and CO_2.

Bipyramidal inclusions that had small fractures extending out from their pointed ends before heating (Fig. 5a) were partially (Fig. 5b) or completely homogenized, depending upon the experimental conditions. The small, dark-colored cracks are colorless and marked by tiny gas bubbles after heating (see also Fig. 6c).

Results of spectroscopic analysis of homogenized and unheated inclusions

Spectroscopic analyses for H_2O and CO_2 for homogenized inclusions are in Table 2. The results are compared to those of stratigraphically equivalent, unheated, glassy or partly devitrified inclusions in Figure 7 for H_2O and Figure 8 for CO_2. The nine homogenized plinian inclusions include seven variably devitrified inclusions from pumice clast 6B and two inclusions from pumice sample 21A that were clear and glassy and free of vapor bubbles before heating. Analyses range from 4.92 to 5.88 wt% H_2O (total) and ~70–180 ppm CO_2. H_2O concentrations of these heated inclusions are within the range (5.31–6.83 wt%) of H_2O concentrations measured for stratigraphically equivalent unheated clear glass or green glass (slightly devitrified) plinian inclusions, with one exception (4.92 wt%) (Fig. 7A). The unheated plinian inclusions represented in Figure 7A comprise 37 glassy inclusions from 11 pumice clasts collected from different stratigraphic levels within the plinian ash-fall pumice deposit. CO_2 concentrations of homogenized inclusions are also within the measured range of CO_2 concentrations for unheated inclusions (30–240 ppm) (Fig. 8A).

Analyses of 11 homogenized inclusions from the low temperature Chidago and Gorges ash-flow units yielded H_2O concentrations ranging from 4.96 to 6.24 wt% and CO_2 from 30 to 210 ppm. The concentrations for homogenized Chidago inclusions, as well as homogenized Gorges inclusions, overlap the low end of the range of values measured for unheated, clear glass or green glass inclusions from the Chidago lobe (20 inclusion analyses from six pumice samples: 5.3–7.0 wt% H_2O, 20–370 ppm CO_2; see Figs. 7B and 8B). No glassy inclusion analogues exist in the Gorges pumices used for this study. However, we believe that the comparison of heated Gorges inclusions to unheated Chidago inclusions is reasonable because the early ash-flow units are closely related in eruptive history, Fe-Ti oxide quench temperatures, and mineral content (Hildreth, 1979).

Homogenized inclusions from the Mono Basin ash flow have the lowest measured H_2O concentrations (3.72–4.59 wt%) and span the largest range in CO_2 (~10–660 ppm) (see Figs. 7C and 8C). The 20 glass inclusions analyzed are from five pumice clasts and nine of the inclusions are from one pumice clast, LV81-17A. The CO_2 concentra-

TABLE 1. Experimental data for successfully homogenized glass inclusions in quartz phenocrysts from the Bishop Tuff

Inclusion	T (°C)	P (kbar)	t (h)	Inclusion texture before heating*
				Plinian deposit
6B-1**	800	2.2	21	gg, slight speckled devitrified (cloudy glass), n, r
6B-2	800	2.2	21	gg, slight speckled devitrified (cloudy glass), n, r
6B-4	800	2.2	21	gbg, slight speckled devitrified (cloudy glass), b, r
6B-G5	800	2.0	20.5	bg, speckled devitrified (cloudy glass), n, r
6B-G61	800	2.0	20.5	bg, speckled devitrified (cloudy glass), n, r-pf
6B-G62	800	2.0	20.5	bg, speckled devitrified (cloudy glass), b, r-pf
6B-G8	800	2.0	20.5	bg, speckled devitrified (cloudy glass), n, r-pf
21A-31	800	2.0	20	g, n, r-pf
21A-32	800	2.0	20	g, n, r-pf
				Chidago lobe
10-1	800	2.0	20	g, n, r
10-2	800	2.0	20	g, n, r
13	800	2.2	21	gg, n, r
16-H5	800	2.0	20.5	opaque, birefringent crystalline rim, pf
16-H61	800	2.0	20.5	opaque, pf
16-H62	800	2.0	20.5	opaque, pf
				Gorges lobe
24-C3	800	2.0	20.5	opaque, pf
133A-1	800	2.2	22	coarse-grained dark crystals along walls; coarse, colorless crystals + b interior, r
133A-2	800	2.2	22	opaque, pf-f
133A-7	800	2.2	22	coarse-grained dark crystals along walls; coarse, colorless crystals + b interior, pf
133A-10	800	2.0	10	coarse-grained dark crystals along walls; coarse, colorless crystals + b interior, pf
				Mono Basin lobe
32W-1†	900	2.2	24	opaque, pf
32W-41†	900	2.2	24	opaque, r-pf
32W-42†	900	2.2	24	opaque, r-pf
32W-5†	900	2.2	24	opaque, r-pf
41-2‡	900	2.2	24	opaque, small, dark (glass-filled?) cracks at the ends of inclusion, f
41-3‡	900	2.2	24	opaque, f
42-3‡	900	2.2	24	opaque, small, dark (glass-filled?) cracks at the ends of inclusion, pf
42-5‡	900	2.2	24	opaque, small, dark (glass-filled?) cracks at the ends of inclusion, f
42-6‡	900	2.2	24	opaque, small, dark (glass-filled?) cracks at the ends of inclusion, f
45-3‡	900	2.2	24	opaque, small, dark (glass-filled?) cracks at the ends of inclusion, f
45-4‡	900	2.2	24	opaque, f
LV81-17A-1	800	2.0	20	g, slight speckled devitrified, b, extremely f
LV81-17A-2	800	2.0	20	g, slight speckled devitrified, several b with attached crystals, f
LV81-17A-31§	900	2.2	24	g, speckled devitrified, several b with attached crystals, pf
LV81-17A-32§	900	2.2	24	g, speckled devitrified, several b with attached crystals, pf
LV81-17A-51	800	2.0	20	g, speckled devitrified, b, pf
LV81-17A-52	800	2.0	20	g, speckled devitrified, b, pf
LV81-17A-61	800	2.0	20	g, speckled devitrified, several crystal clusters attached to wall, n?, pf-f
LV81-17A-62	800	2.0	20	g, speckled devitrified, two crystal clusters attached to wall, n?, pf
LV81-17A-7	800	2.0	20	g, slight speckled devitrified, b, extremely f

* gg = green glass; gbg = green-brown glass; bg = brown glass; g = clear, colorless glass; n = no vapor bubble; b = vapor bubble; r = rounded inclusion; pf = partly faceted inclusion; f = faceted (negative-crystal) inclusion.

** Number (with or without letter) before hyphen is pumice label; number after hyphen is inclusion label.

† Shown are the experimental conditions of the third (final) experiment. Inclusions were previously heated twice at 800 °C, 2.0 kbar for 20 h (40 h total). The initial experiment at 800 °C resulted in partial homogenization with the inclusions retaining a birefringent polycrystalline core, tiny crystals (1–5 μm) interior or along the wall and vapor bubbles embedded in the inclusion wall. Little or no change resulted after the second experiment. After the final experiment, inclusions are completely glassy except for a few tiny crystals along a slightly bumpy inclusion wall. No vapor bubbles remain.

‡ Shown are the experimental conditions of the second (final) experiment. Inclusions were previously heated at 805 °C, 2.2 kbar for 24 h, which resulted in partial homogenization as described in note †. After the second experiment, inclusions are completely glassy except for a few tiny crystals along a slightly bumpy inclusion wall. No vapor bubbles remain. Inclusion 45-4 has a fairly smooth wall and no crystals remaining. Inclusions 41-2, 42-3, 42-5, 42-6, and 45-3 have small cracks at the ends of the inclusion that are colorless and marked by tiny vapor bubbles after heating.

§ Shown are the experimental conditions of the second (final) experiment. Inclusions were previously heated at 800 °C, 2.0 kbar for 20 h, which resulted in nearly complete homogenization, except for a few tiny birefringent crystal clusters ($\leq$10 μm) remaining attached to a smooth wall; no vapor bubbles remain. After the second experiment, most crystals remain but are small in size.

tions of these nine inclusions vary widely from crystal to crystal, ranging from 180 to 660 ppm. Two unheated inclusions containing vapor bubbles and slight devitrification from the same pumice clast (LV81-17A) were analyzed spectroscopically by Anderson et al. (1989), along with two other similar-looking inclusions from pumice clast LV81-18A. In order to account for the gas content of the bubbles in these inclusions, they calculated an amount of gas in the bubble by assuming that the bubble equilibrated with the melt at the preeruption temperature and the saturation pressure inferred for the glass. The amount of gas calculated to be in the bubble was then added to the spectroscopically measured amounts of H_2O and CO_2 in the glass to get a restored primary bulk volatile composition of the inclusion. The restored values of Anderson et al. (1989) are labeled in Figures 7C and 8C as the unheated values. The restored H_2O and CO_2 contents of the inclusions from Anderson et al. (1989) in Table 3 are similar to the values measured for similar-looking (i.e., similarly devitrified) but homogenized inclusions produced in this study (Table 2).

A selection of colorless and green glassy (± vapor bub-

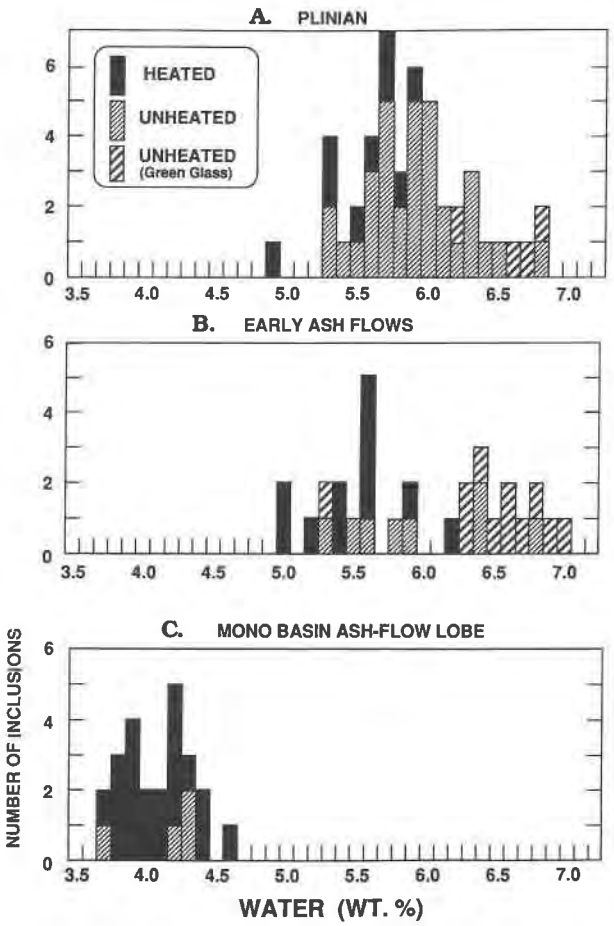

Fig. 7. Frequency diagram showing the distribution of H_2O (as the sum of H_2O_{mol} + OH^- as H_2O in wt%) determined by spectroscopic analysis for unheated (naturally colorless, or green glassy) and heated inclusions from the (**A**) plinian air-fall pumice unit, (**B**) early ash flows: Chidago and Gorges ash-flow lobes (all of the unheated inclusions shown in **B** are from the Chidago lobe only), (**C**) Mono Basin ash-flow lobe. The four unheated analyses for the Mono Basin lobe are from partly devitrified inclusions containing crystallites and vapor bubbles and represent the restored primary bulk volatile compositions taken from Anderson et al. (1989) and listed in Table 3. H_2O concentrations were rounded to the nearest tenth of a weight percent for plotting. (For example, the 5.0 wt% interval contains all inclusions with concentrations ranging from 4.95 to 5.04 wt%.)

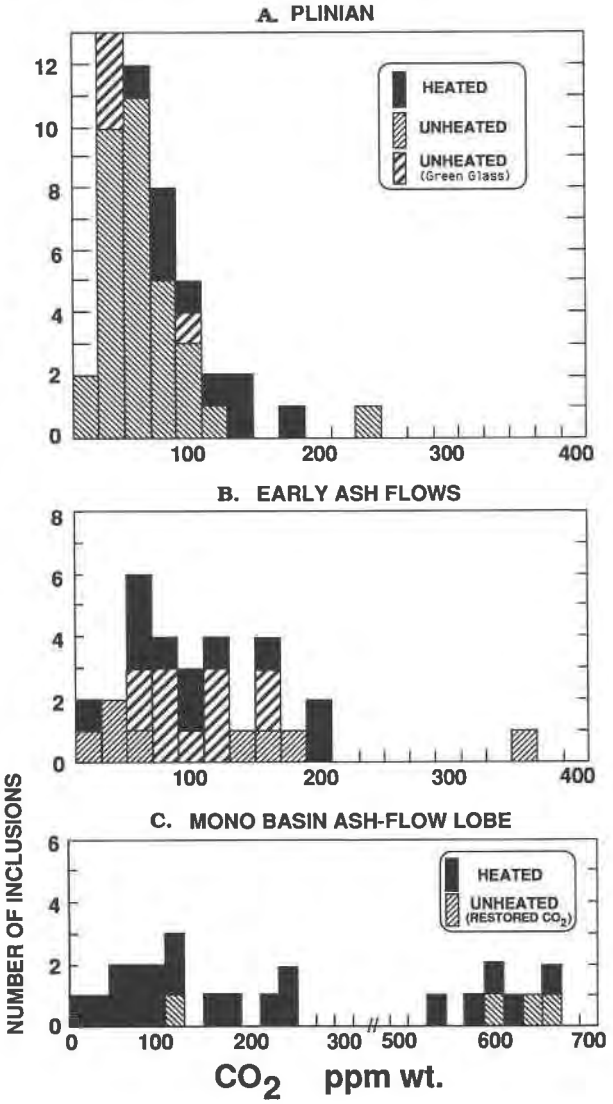

Fig. 8. Frequency diagram showing the distribution of CO_2 (ppm wt) determined by spectroscopic analysis for unheated (naturally colorless, or green glassy) and heated inclusions from the (**A**) plinian air-fall pumice unit, (**B**) early ash flows: Chidago and Gorges ash-flow lobes (all of the unheated inclusions shown in **B** are from the Chidago lobe only), (**C**) Mono Basin ash-flow lobe. Note concentration scale change in **C**. The four unheated analyses for the Mono Basin lobe are from partly devitrified inclusions containing crystallites and vapor bubbles and represent the restored primary bulk volatile compositions taken from Anderson et al. (1989) and listed in Table 3. Concentrations were rounded to nearest tens of ppm for plotting in 20-ppm intervals. (For example, the interval at 100 ppm contains all inclusions with concentrations ranging from 91 to 110 ppm.)

bles) inclusions from plinian ash-fall pumice and Chidago ash-flow pumice were heated to compare measured H_2O and CO_2 with unheated inclusions from the same pumice samples. These comparisons are shown in Figure 9 for H_2O and Figure 10 for CO_2. Spectroscopic analyses for H_2O and CO_2 for the unheated inclusions are in Table 3. Each pumice sample consists of either a single pumice clast (as for pumice samples 6B, LV81-17A, and LV81-18A) or several pumice clasts taken from the same stratigraphic level within an eruptive unit (pumice samples 21A, plinian; 10, 13, and 16, Chidago). The unheated inclusions from these pumices are clear or colored glass, with or without a vapor bubble. The inclusions chosen for heating were either texturally similar or somewhat more extensively devitrified than the unheated counterparts, as noted in the legend for each pumice sample in Figure 9. H_2O concentrations of the selected heated inclusions (first 15 analyses of Table 2) are on average about

1 wt% lower than unheated inclusions from the same samples. As shown in Figure 10, CO_2 concentrations of heated inclusions display no systematic variation with unheated inclusions; i.e., the heated values are either slightly lower or higher than the unheated values.

Although presentation and discussion of petrologic variations in H_2O and CO_2 for the Bishop Tuff is reserved for a later publication (Skirius, in preparation), it is relevant to note that the concentrations of H_2O and CO_2 in inclusions vary as much within as between pumice clasts from the same stratigraphic levels (Tables 2 and 3; see also Skirius, 1989). This is true for subsets of only heated or only unheated inclusions, as well as the combined data sets.

TABLE 2. Results of spectroscopic analyses on homogenized glass inclusions from the Bishop Tuff

Inclusion	$H_2O_{(mol)}$	OH^-	$H_2O_{(total)}$	CO_2	H_2O_{mol}/OH^-
Plinian deposit					
6B-1	4.02	1.59	5.61	102	2.53
6B-2	3.71	1.60	5.31	120	2.32
6B-4	3.68	1.59	5.27	90	2.31
6B-G5	4.12	1.54	5.66	93	2.68
6B-G61	4.00	1.50	5.50	94	2.67
6B-G62	4.30	1.58	5.88	183	2.72
6B-G8	4.15	1.55	5.70	69	2.68
21A-31	4.15	1.61	5.76	136	2.58
21A-32	3.56	1.36	4.92	135	2.62
Chidago lobe					
10-1	4.12	1.50	5.62	100	2.75
10-2	4.05	1.54	5.59	82	2.63
13	3.89	1.55	5.44	60	2.51
16-H5	3.66	1.50	5.16	163	2.44
16-H61	3.57	1.44	5.01	119	2.48
16-H62	3.87	1.52	5.39	198	2.55
Gorges lobe					
24-C3	4.05	1.50	5.55	114	2.70
133A-1	4.67	1.57	6.24	30	2.98
133A-2	3.65	1.31	4.96	213	2.79
133A-7	4.47	1.42	5.89	66	3.12
133A-10	4.14	1.46	5.60	74	2.84
Mono Basin lobe					
32W-1	2.33	1.50	3.83	69	1.55
32W-41	2.53	1.64	4.17	122	1.54
32W-42	2.21	1.56	3.77	65	1.42
32W-5	2.43	1.49	3.92	75	1.63
41-2	2.56	1.34	3.90	45	1.91
41-3	2.55	1.54	4.09	76	1.66
42-3	2.89	1.53	4.42	107	1.89
42-5	2.51	1.58	4.09	96	1.59
42-6	2.67	1.49	4.15	117	1.79
45-3	2.36	1.49	3.85	158	1.58
45-4	2.39	1.33	3.72	13	1.80
LV81-17A-1	2.68	1.34	4.02	182	2.00
LV81-17A-2	3.01	1.58	4.59	550	1.91
LV81-17A-31	2.52	1.38	3.90	586	1.83
LV81-17A-32	2.46	1.36	3.82	661	1.81
LV81-17A-51	2.85	1.46	4.31	254	1.95
LV81-17A-52	2.73	1.48	4.21	224	1.85
LV81-17A-61	2.71	1.53	4.24	616	1.77
LV81-17A-62	2.89	1.50	4.38	611	1.93
LV81-17A-7	2.55	1.46	4.01	254	1.75

Note: Measured species for H_2O (H_2O total is given as the sum of H_2O_{mol} and OH^- as H_2O) in wt%; CO_2 in ppm wt.

Discussion

Effect of cracks on homogenization of melt inclusion

The behavior of inclusions with respect to heating varies in accord with a variety of cracks and associated features that are evident in the preheated samples. These variations can be related to the probable temperatures of initial cracking and consequent volatile loss and induced crystallization, as discussed below.

Penetrative cracks. Devitrification products of inclusions intersected by a penetrative crack in the quartz host (passing from the exterior of the crystal to the inclusion) prior to heating do not dissolve to a homogeneous glass but remain unaffected after the heating procedure, as previously noted. An example of a quartz crystal containing devitrifed inclusions intersected by a visible crack is shown in Figure 4. Because other uncracked devitrifed inclusions within this same crystal were homogenized, the cracked inclusions must have lost volatiles by diffusion along the crack, either during the experiment or, more likely, during natural cooling and devitrification. Similar observations for cracked, devitrified inclusions were made by Lemmlein et al. (1962) and Takenouchi and Imai (1975) in heating experiments on inclusions in topaz and quartz, respectively. The apparent inability of devitrified inclusions in sanidine crystals to revitrify may also be explained by diffusional loss of H_2O along cleavage cracks.

Rare glassy inclusions containing several large vapor bubbles, as shown in Figure 5f, also could not be homogenized in the experiments. The bubbles remained unchanged in size, shape, and position after being heated. Although it is not apparent in the figure, these inclusions are also intersected by a crack in the quartz crystal. In this case, cracking very likely occurred early in the cooling history at elevated temperature, while the melt is fluid enough to allow bubble nucleation and expansion. The likely result is dehydration of the inclusion by escape of H_2O along the crack. Lack of devitrification in such vesiculated glassy inclusions in ash-flow crystals containing other extensively devitrified (opaque) inclusions suggests that the glassy inclusions were unable to devitrify because they were H_2O-poor, like the glass adhering to the surfaces of the quartz crystals.

Single vapor bubbles in glassy inclusions, uncommon in the early-erupted plinian and ash-flow samples, do not result from cracks in the surrounding quartz. The size of the bubble ($< \sim 0.5$ vol% of inclusion) correlates well with inclusion size and is thought to be due to shrinkage of the melt during cooling, either before or during eruption, or during quenching (Anderson et al., 1989). Some plinian ash-fall crystals that contained initially uncracked inclusions with one or, more rarely, two shrinkage bubbles developed cracks or broke into pieces as a result of heating. This may suggest that the vapor bubbles in these inclusions contained a significant amount of gas, which became overpressurized upon rapid heating and caused cracking. This behavior contrasts with the survival during heating of bubble-bearing inclusions from late, high-T Mono Basin ash-flow samples LV81-17A and LV81-18A. The bubbles in these partially devitrified inclusions were predicted by Anderson et al. (1989) to contain a gas rich

TABLE 3. Results of spectroscopic analyses on unheated (natural) glass inclusions from the same Bishop Tuff pumice samples as heated inclusions in Table 2

Inclusion	$H_2O_{(mol)}$	OH^-	$H_2O_{(total)}$	CO_2	H_2O_{mol}/OH^-	Notes*
			Plinian deposit			
6B-D2	5.79	1.04	6.83	102	5.57	gg, n
6B-D3-1	5.74	0.99	6.73	49	5.24	gg, xl, n
6B-D3-2	5.55	1.05	6.60	49	5.64	gg, xl, n
6B-D3-3	5.30	0.88	6.18	50	5.53	gg, xl, n
21A-2	5.19	1.15	6.34	102	4.51	g, n
21A-C8	5.54	1.29	6.83	51	4.29	g, b
21A-C11	4.91	1.14	6.05	43	4.31	g, b
21A-8-1	5.00	1.03	6.03	45	4.85	g, b
21A-8-2	4.95	1.04	5.99	41	4.76	g, n
21A-LU	4.74	1.12	5.86	44	4.23	g, n
			Chidago lobe			
10-LUA	5.70	1.10	6.80	142	5.18	g, n
10-LUB	5.88	1.06	6.94	121	5.55	gg, n
13-E7-1	5.52	1.03	6.55	115	5.36	gg, n
13-E7-2	5.67	1.08	6.75	106	5.25	gg, n
13-LU-1	5.64	0.95	6.59	85	5.94	gg, n
13-LU-3	4.23	1.11	5.34	72	3.81	gg, b
16-LU	5.38	1.05	6.43	161	5.12	gg, n
			Mono Basin lobe			
LV81-17A-5**	3.4	0.9	4.3	600	3.78	g, xl, b
LV81-17A-6**	3.1	0.7	3.8	115	4.43	g, xl, b
LV81-18A-5**	3.4	0.9	4.3	660	3.78	g, xl, b
LV81-18A-11**	3.3	0.9	4.2	635	3.67	g, xl, b

Note: Measured species for H_2O (H_2O total is given as the sum of H_2O_{mol} and OH^- as H_2O) in wt%; CO_2 in ppm wt.

* g = colorless glass; gg = green glass; n = no vapor bubble; b = vapor bubble; xl = few birefringent crystals.

** Values taken from Anderson et al. (1989); H_2O and CO_2 concentrations are restored values (i.e., gas calculated to be in vapor bubbles is added to spectroscopically measured volatile concentrations to get a restored bulk volatile composition for the inclusion).

in CO_2, which would significantly increase the total CO_2 content of the inclusions.

Localized cracks resulting from the β-α inversion of quartz. Many large devitrified inclusions from the high-T ash flows were noted to have cracks radiating short distances from the apices of the inclusion into the quartz host. The cracks are subparallel to the **c** axis of the host and are likely to have originated from the sudden 1 vol% shrinkage of quartz on cooling thorugh the β-α inversion at ~573 °C (Ghiorso et al., 1979; Roedder, 1984). Inclusions with these cracks (Figs. 3b, 5a) were partially (Fig. 5b) or completely (Fig. 3f) homogenized, depending upon the experimental conditions. The small cracks that were dark-colored before heating become colorless, and some are marked by tiny gas bubbles after heating (Figs. 5b, 6c). The revitrification of such inclusions is interpreted to signify that this type of cracking is localized such that little or no H_2O escaped from the inclusion. If much H_2O had escaped, then the crystallites would quite likely remain with heating, as is commonly observed for most devitrified inclusions with penetrative cracks.

Rapid laboratory cooling through the β-α inversion may cause the crystal to be strained adjacent to the heated inclusions. A stressed region around an inclusion explains the cracks that commonly develop during polishing of heated inclusions.

Cracking of host minerals is more prevalent for more slowly cooled materials (ash flows). Depending upon the temperature of cracking, the inclusion may be preserved as a vesicular glass (high T) or as a heavily devitrified or crystallized inclusion with a diminished volatile content. Although some of these may be revitrified by heating, they may be low in volatiles. Evidently, many ash-flow inclusions have lost volatiles during posteruptive cooling. Our comparative studies reveal that devitrified inclusions that lack cracks and some with tiny nonpenetrative cracks have preserved their initial volatile concentrations, and some of these can be revitrified without volatile loss.

It is likely that retention of volatiles is favored by natural preservation of a high proportion of residual glass, because crystallization (devitrification) in a confined volume results in considerable internal overpressures (easily on the order of several kilobars if the volatiles are rich in H_2O). Consequently, studies of volatiles in melt inclusions should selectively emphasize glass-rich, uncracked inclusions.

Effect of homogenization experiments on glass inclusions

Volatile concentrations. Comparison of H_2O concentrations for heated and unheated inclusions from the same clast or stratigraphically equivalent clasts of early-erupted, plinian and Chidago lobe pumice shows that the heated inclusions have an average of about 1.0 wt% less H_2O than their unheated counterparts (Fig. 9). The difference of ~1 wt% is not likely to be due to loss of H_2O, possibly as H_2, during artificial heating for the following reasons: (1) Heated inclusions yield H_2O concentrations that show less variability than those of the larger group of stratigraphically equivalent naturally glassy inclusions (see Fig. 7). If H_2O were lost by diffusion during heating, then afterward we would expect greater variation in H_2O concentrations related to variable quartz thickness and size

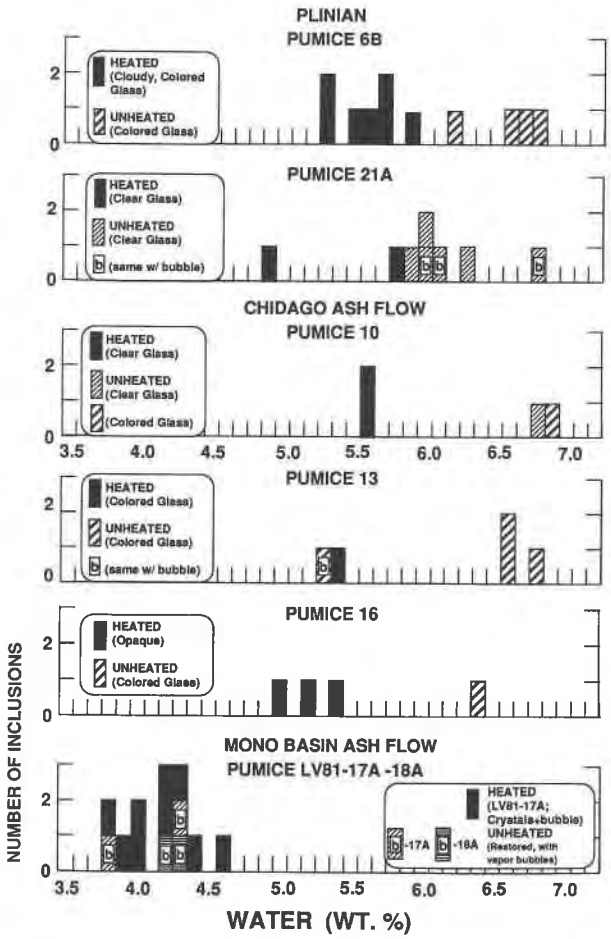

Fig. 9. Frequency diagram showing the distribution of H_2O (as the sum of H_2O_{mol} + OH^- as H_2O in wt%) determined by spectroscopic analysis for unheated and heated inclusions from the same pumice samples. Pumice samples 6B, LV81-17A, and LV81-18A each consists of a single pumice clast; pumice samples 21A, 10, 13, and 16 each consists of one or more individual pumice clasts that are stratigraphically equivalent. Inclusion textures before heating are noted in figure legends and also in Tables 1 and 3. H_2O concentrations were rounded to the nearest tenth of a weight percent for plotting as in Figure 7.

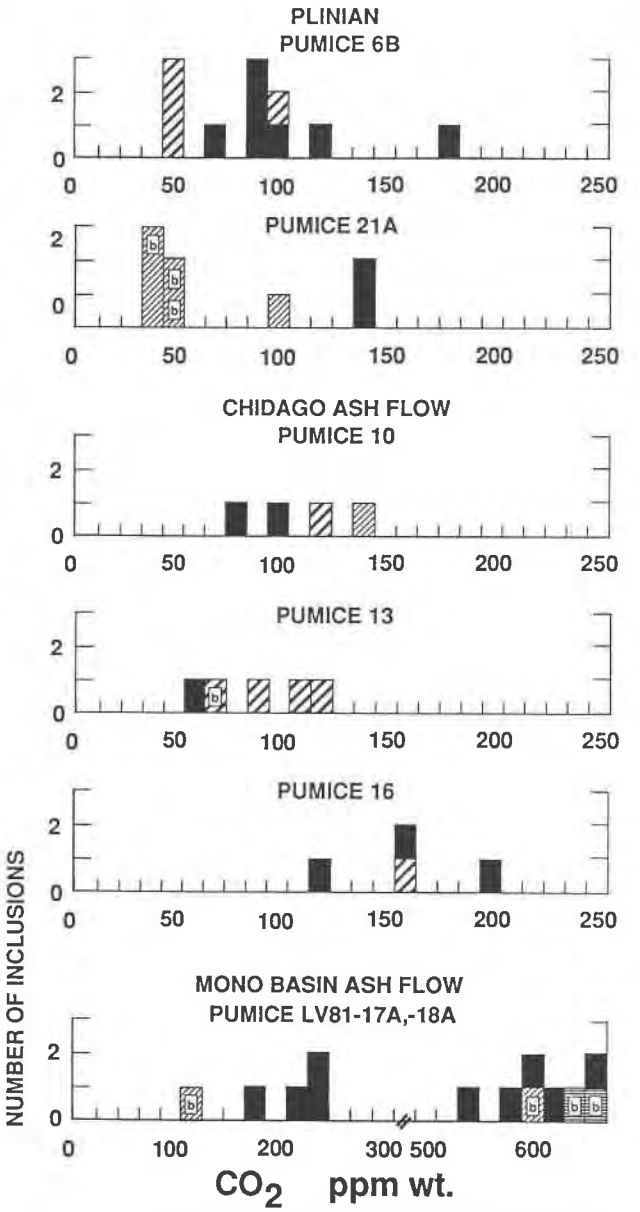

Fig. 10. Frequency diagram showing the distribution of CO_2 (ppm wt) determined by spectroscopic analysis for unheated and heated inclusions from the same pumice samples. Notes on samples and inclusion textures before heating are noted in figure legends of Figure 9 and also in Tables 1 and 3. Concentrations were rounded to nearest tens of ppm for plotting in 10-ppm intervals (20-ppm intervals for Mono Basin ash flow; see caption to Fig. 8).

of inclusion. (2) The inclusions are free of magnetite, which would be expected to crystallize if H_2 were lost. The natural green or brown coloration of some glassy inclusions from the Toba Tuff has been attributed to the effects of partial oxidation resulting from loss of H_2 by Beddoe-Stephens et al. (1983). Although some inclusions were colored before heating, afterward they are colorless. Diffusion of H_2 into the inclusion during heating is unlikely because the partial pressure of H_2O in the Ar gas medium surrounding the crystal was very low. The coloration is likely caused by dispersed crystallites, as was also concluded by Takenouchi and Imai (1975) when their colored glass inclusions lost color after being heated.

The reason for the lower H_2O concentrations for the heated early-erupted, plinian and Chidago inclusions (compared with unheated counterparts) is not certain at this time. Heated inclusions were compared to unheated inclusions from the same or similar pumice clasts based on the assumption that such inclusions would have had the same or closely similar posteruptive cooling histories. The rate of posteruptive cooling was considered to have a strong influence on the extent of devitrification and glass inclusion texture. However, based on the observation that

even inclusions (uncracked) in different crystals from the same plinian pumice clast (6B) have varied amounts of devitrification, it is likely that devitrification is influenced by volatile content. Major element compositions do not vary significantly between heated and unheated inclusions from 6B and all other analyzed samples (Skirius, unpublished data). Comparisons of H_2O and CO_2 between heated and unheated variably devitrified inclusions from sample 6B may, in fact, reveal a natural variation in melt volatile content (Figs. 9 and 10) that could result from differentiation.

When the comparison is made for texturally similar inclusions (before heating) from the same Mono Basin pumice clast (LV81-17A), as well as for unheated inclusions from LV81-18A, volatile concentrations are similar. Likewise, it follows that similarly devitrified inclusions from the same pumice clast (i.e., inclusions that have experienced an identical rate of posteruptive cooling) are similar in volatile content. Comparison of texturally similar inclusions from multiple pumice clast samples (pumices 21A, 10, and 13) shows that heated and unheated H_2O concentrations are different, and any relation between texture and volatile content is inconclusive.

Lower H_2O concentrations for heated inclusions for most samples may suggest that there is an analytical artifact involved in determining the H_2O content of unheated glassy or colored glassy inclusions that reflects an effect of the cooling history or devitrification process of natural glass inclusions on the molar absorptivities. Newman et al. (1986) and Silver et al. (1990) used obsidian glasses and rapidly quenched synthetic glasses (cooling rates ~200 °C/s), respectively, to determine molar absorptivities of the H_2O_{mol} and OH^- IR bands for rhyolitic glasses containing up to ~4.0 wt% total H_2O. It may be that most pumice from plinian and nonwelded ash-flow deposits did not cool quickly enough to make glassy inclusions in these materials essentially equivalent to experimentally quenched glasses with regard to molar absorptivities for H_2O. High H_2O_{mol}/OH^- ratios (see Table 3) as measured for most unheated inclusions (especially green glassy inclusions with the highest measured total H_2O concentrations; see Figs. 7A and 7B) may indicate slow cooling for these inclusions (Stolper, 1989). In addition, the green color of some of these inclusions may reflect a reorganization of the glass (clustering of H_2O molecules?) as part of incipient devitrification during cooling. Although the heated inclusions are more slowly cooled than the experimental hydrous glasses of Silver et al. (1990), the measured H_2O_{mol}/OH^- ratios are similar to some experimental glasses with similar total H_2O contents and are consistent for their homogenization quench temperature (Stolper, 1989).

Dissolution of devitrification products. The homogenization process involves bringing a devitrified inclusion back to the *P-T* conditions under which it was trapped as a homogeneous melt containing dissolved magmatic volatiles. The crystalline phases of uncracked, devitrified inclusions should dissolve (along with gas bubbles present because of melt contraction or shrinkage) as the temperature and pressure are brought to near liquidus conditions. H_2O present in hydrous crystals or residual glass facilitates melting by lowering the liquidus temperature and melt viscosity, which helps to overcome the metastability commonly encountered in silicic systems. The higher heating temperature (900 °C) necessary for homogenization of most Mono Basin inclusions probably helped to overcome the sluggish re-solution of daughter minerals in these highly devitrified, lower H_2O inclusions. Inclusions retaining few, highly refractive tiny crystals along the wall of otherwise revitrified inclusions suggests a sluggish approach to equilibrium (Roedder, 1984, p. 100–101). This may be the case for the uncracked Adobe Valley inclusions. If they have lower H_2O contents than the Mono Basin inclusions (most of which were homogenized at 900 °C), then an experimental temperature >900 °C may homogenize them.

Protruding bubbles in incompletely homogenized inclusions

Partially homogenized inculsions, as shown in Figure 6, retained crystals and vapor bubbles that protrude ~6–14 μm into the surrounding quartz from an irregular, bumpy inclusion wall. An interesting explanation for the protruding bubbles is that given by Donaldson and Henderson (1988) for the formation of rounded embayments in quartz crystals. As a bubble nears the dissolving quartz wall it enters a compositional boundary layer in the melt. The part of the bubble nearest the crystal will be in contact with the most SiO_2-rich melt having the largest surface tension. The nonuniform surface tension of the melt around the bubble causes instability and results in small-scale convection of the melt about the bubble (Marangoni convection). Convective flow removes SiO_2-rich melt at the interface between the bubble and the quartz host and replaces it with less siliceous, more undersaturated melt, thereby locally enhancing the dissolution rate of the quartz ahead of the bubble. The bubble apparently drills its way into the quartz. Approximately 5 μm of dissolution associated with the bubbles should have occurred during our experiments, in accordance with the estimated dissolution rate of quartz (~0.2 μm/h) given by Donaldson and Henderson (1988). This is approximately the amount of bubble protrusion most commonly observed.

Another explanation for the embedded bubbles might be that following bubble localization on the inclusion wall, 6–14 μm of quartz growth from the wall inward embedded the bubbles. However, a layer of quartz growth 6 μm thick along the wall of a spherical inclusion 100 μm in diameter initially containing 4 wt% H_2O would result in ~32% crystallization of the inclusion volume and an increase in H_2O content of 1.88 wt%. We do not observe high H_2O concentrations for such inclusions that were subsequently homogenized at higher temperature. In addition, the diameter of the partially vitrified inclusions (excluding the amount of bubble protrusion) did not de-

crease by 6–14 μm compared to the diameter of the devitrified inclusions (before heating), as accurately as can be determined for opaque inclusions. Furthermore, the temperature of the experiment is approximately 100 °C above the H_2O-saturated liquidus temperature for rhyolitic melt (interpolated from the data of Tuttle and Bowen, 1958), which would favor quartz dissolution, not crystallization. Again, however, inclusion diameter did not increase.

The irregular inclusion outline and overall bumpiness of the inclusion wall is likely due to a small amount of natural quartz precipitation during devitrification. This quartz growth remained apparently unaffected after heating at 800 °C but was partially dissolved at 900 °C (the wall became less bumpy). Because the walls remained slightly bumpy even at 900 °C, not all of the secondary quartz was dissolved to an assumed original smooth wall, and therefore the measured volatile concentrations may be considered maximum values for these inclusions.

Conclusions

It is possible to homogenize many variably devitrified glass inclusions in quartz phenocrysts from the Bishop Tuff. Volatile loss during heating appears negligible, but many inclusions have lost volatiles through cracks during natural cooling. Homogenized inclusions, although in thermally stressed quartz, can be doubly polished and used for spectroscopic studies of melt volatiles, as well as for other melt compositional studies requiring glassy samples.

Some heated inclusions appear to have ~1.0 wt% less H_2O than their glassy or partly devitrified counterparts. Loss of significant amounts of H_2O during heating is unlikely. Rather, experimentally quenched glass inclusions have a thermal history more similar to experimental glasses upon which the spectroscopic calibration for H_2O is based. Therefore, our experimentally quenched inclusions probably yield the most accurate H_2O concentrations. Additional studies, perhaps using other analytical techniques, of inclusions before and after heating are needed to unravel apparent losses during heating from possible temperature effects on spectroscopic calibration for H_2O.

Acknowledgments

This study was supported by Department of Energy Contract ER10763 and National Science Foundation Grant 89-04070 to Anderson. We thank Robert Newton for use of experimental lab facilities at the University of Chicago (NSF EAR-8707156) and Ed Stolper, George Rossman, and Sally Newman for use of the FTIR lab at Caltech and for helpful advice. The manuscript has benefited from reviews by N.W. Dunbar, T.A. Vogel, and C.R. Bacon.

References cited

Anderson, A.T., Jr., and Skirius, C.M. (1989) Pre-eruptive CO_2 in Kilauean glass inclusions. IAVCEI General Assembly on Continental Magmatism, New Mexico Bureau of Mines and Mineral Resources, Bulletin 131, 6.

Anderson, A.T., Jr., Newman, S., Williams, S.N., Druitt, T.H., Skirius, C., and Stolper, E. (1989) H_2O, CO_2, Cl, and gas in Plinian and ash-flow Bishop rhyolite. Geology, 17, 221–225.

Bacon, C.R., Newman, S., and Stolper, E. (1988) Preeruptive volatile content, climatic eruption of Mount Mazama, Crater Lake, Oregon. Geological Society of America, Abstracts with Programs, 20, 248.

——— (1990) Water, CO_2, Cl and F contents of glass inclusions in phenocrysts from three Holocene explosive eruptions, Crater Lake, Oregon. V.M. Goldschmidt Conference Program and Abstracts, The Geochemical Society, 29.

Bailey, R.A., Dalrymple, G.B., and Lanphere, M.A. (1976) Volcanism, structure, and geochronology of Long Valley Caldera, Mono County, California. Journal of Geophysical Research, 81, 725–744.

Beddoe-Stephens, B., Aspden, J.A., and Shepherd, T.J. (1983) Glass inclusions and melt compositions of the Toba Tuffs, Northern Sumatra. Contributions to Mineralogy and Petrology, 83, 278–287.

Clocchiatti, R. (1975) Glassy inclusions in crystals of quartz; optical, thermo-optical and chemical studies, and geological applications. Societe Geologique de France Memoires, New Series, 54, 122.

Donaldson, C.H., and Henderson, C.M.B. (1988) A new interpretation of round embayments in quartz crystals. Mineralogical Magazine, 52, 27–33.

Fine, G., and Stolper, E. (1985) The speciation of carbon dioxide in solium aluminosilicate glasses. Contributions to Mineralogy and Petrology, 91, 105–121.

Getting, I.C., and Kennedy, G.C. (1970) Effect of pressure on the emf of chromel-alumel and platinum-platinum 10% rhodium thermocouples. Journal of Applied Physics, 41, 4552–4562.

Ghiorso, M.S., Carmichael, I.S.E., and Moret, L.K. (1979) Inverted high-temperature quartz. Unit cell parameters and properties of the α-β inversion. Contributions to Mineralogy and Petrology, 68, 307–323.

Hildreth, E.W. (1977) The magma chamber of the Bishop Tuff: Gradients in temperature, pressure and composition, 328 p. Ph.D. thesis, University of California.

——— (1979) The Bishop Tuff: Evidence for the origin of compositional zonation in silicic magma chambers. Geological Society of America Special Paper 180, 43–75.

Holloway, J.R. (1971) Internally heated pressure vessels. In G.C. Ulmer, Ed., Research techniques for high pressure and high temperature, p. 217–258. Springer-Verlag, New York.

Karsten, J.L., Holloway, J.R., and Delaney, J.R. (1982) Ion microprobe studies of water in silicate melts: Temperature-dependent water diffusion in obsidian. Earth and Planetary Science Letters, 59, 420–428.

Kozlowski, A. (1981) Melt inclusions in pyroclastic quartz from the Carboniferous deposits of the Holy Cross Mts, and the problem of magmatic corrosion. Acta Geologica Polonica, 31, 273–283.

Lemmlein, G.G., Lliya, M.O., and Ostrovskii, I.A. (1962) The conditions for formation of minerals in pegmatites according to data on primary inclusions in topaz. Akademiia Nauk SSSR, Doklady, 142, 81–83 (translated in Soviet Physics Doklady, 7, 4–6).

Newman, S., Stolper, E.M., and Epstein, S. (1986) Measurement of water in rhyolitic glasses. Calibration of an infrared spectroscopic technique. American Mineralogist, 71, 1527–1541.

Newman, S., Epstein, S., and Stolper, E.M. (1988) Water, carbon dioxide, and hydrogen isotopes in glasses from the ca. 1340 A.D. eruption of the Mono Craters, California: Constraints on degassing phenomena and initial volatile content. Journal of Volcanology and Geothermal Research, 35, 75–96.

Nicolet Operations Manual (1986) Nicolet Analytical Instruments. Madison, Wisconsin.

Payette, C., and Martin, R.F. (1986) The Harvey Volcanic Suite, New Brunswick. I. Inclusions of magma in quartz phenocrysts. Canadian Mineralogist, 24, 557–570.

Roedder, E. (1979) Origin and significance of magmatic inclusions. Bulletin of Mineralogy, 102, 487–510.

——— (1984) Fluid Inclusions. In Mineralogical Society of America Reviews in Mineralogy, 12, 644 p.

Silver, L.A., and Stolper, E. (1989) Water in albitic glasses. Journal of Petrology, 30, 667–709.

Silver, L.A., Ihinger, P.D., and Stolper, E.M. (1990) The influence of bulk composition on the speciation of water in silicate glasses. Contributions to Mineralogy and Petrology, 104, 146–162.

Skirius, C.M. (1989) Pre-eruptive H_2O and CO_2 in Plinian and early ash-flow magma of the Bishop Tuff. IAVCEI General Assembly on Continental Magmatism, New Mexico Bureau of Mines and Mineral Resources, Bulletin 131, 245.

Sobolev, V.S., Bazarova, T.Yu., and Bakumenko, I.T. (1972) Crystallization temperature and gas phase composition of alkaline effusives as indicated by primary melt inclusions in the phenocrysts. Bulletin Volcanologique, 35, 479–496.

Sommer, M.A. (1977) Volatiles H_2O, CO_2, and CO in silicate melt inclusions in quartz phenocrysts from the rhyolitic Bandelier air-fall and ash-flow tuff, New Mexico. Journal of Geology, 85, 423–432.

Stolper, E. (1989) Temperature dependence of the speciation of water in rhyolitic melts and glasses. American Mineralogist, 74, 1247–1257.

Stolper, E., Fine, G., Johnson, T., and Newman, S. (1987) The solubility of carbon dioxide in albitic melt. American Mineralogist, 72, 1071–1085.

Takenouchi, S., and Imai, H. (1975) Glass and fluid inclusions in acidic igneous rocks from some mining areas in Japan. Economic Geology, 70, 750–769.

Tuttle, O.F., and Bowen, N.L. (1958) Origin of granite in the light of experimental studies in the system $NaAlSi_3O8$-$KAlSi_3O8$-SiO_2-H_2O. Geological Society of America Memoir 74.

Watson, E.B., Sneeringer, M.A., and Ross, A. (1982) Diffusion of dissolved carbonate in magmas: Experimental results and applications. Earth and Planetary Science Letters, 61, 346–358.

Manuscript received April 3, 1990
Manuscript accepted September 14, 1990